Optimal diffusion weighting for *in-vivo* cardiac diffusion tensor imaging

Andrew D Scott[1,2], Pedro FADC Ferreira[1,2], Sonia Nielles-Vallespin[1,3], Peter Gatehouse[1,2], Laura-Ann McGill[1,2], Philip Kilner[1,2], Dudley J Pennell[1,2], David N Firmin[1,2].

Affiliations

1. NIHR Cardiovascular Biomedical Research Unit
   Royal Brompton Hospital
   Sydney Street
   London
   SW3 6NP
   UK
2. National Heart and Lung Institute
   Imperial College
   London
   UK
3. National Heart, Lung and Blood Institute
   National Institutes of Health
   Bethesda
   Maryland
   USA

Corresponding Author: Andrew D Scott – a.scott@rbht.nhs.uk, address as 1,.

Key words: DTI; diffusion weighting; b-value; cardiac diffusion; microvascular perfusion

Funding: This work was performed at the National Institute for Health Research Cardiovascular Biomedical Research Unit at The Royal Brompton Hospital and Imperial College London.

Running title: Optimal b-values in cardiac DTI.

Word Count: 4998.

Final published version available at:

http://onlinelibrary.wiley.com/doi/10.1002/mrm.25418/abstract

ABSTRACT

Purpose: To investigate the influence of the diffusion weighting on *in-vivo* cardiac diffusion tensor imaging (cDTI) and obtain optimal parameters.

Methods: 10 subjects were scanned using STEAM-EPI with 6 b-values, from 50 to 950smm^{-2}, plus b=15smm^{-2} reference. The relationship between b-value and both signal loss and signal to noise ratio measures was investigated. Mean diffusivity (MD), fractional anisotropy (FA) and helical angle (HA) maps were calculated using all possible b-value pairs to investigate the effects diffusion weighting of the main and reference data.

Results: Signal decay at low b-values was dominated by processes with high apparent diffusion coefficients, most likely microvascular perfusion. This effect could be avoided by diffusion weighting the reference images. Parameter maps were improved with increased b-value, until the diffusion-weighted signal approached the noise floor. For the protocol used in this study, b=750smm^{-2} combined with 150smm^{-2} diffusion weighting of the reference images proved optimal.

Conclusion: MD, FA and HA from cDTI are influenced by the b-value of the main and reference data. Using optimal values improves parameter maps and avoids microvascular perfusion effects. This optimized protocol should provide greater sensitivity to pathological changes in parameter maps.

Introduction

The ability to interrogate the microstructure of myocardial tissue has led to considerable interest in cardiac diffusion tensor imaging (cDTI) (1, 2, 3, 4, 5, 6, 7, 8, 9, 10, 11, 12, 13, 14). Diffusion-weighted contrast (with magnitude described by the b-value) is the result of signal loss caused by incoherent motion within a mixing time between two diffusion-encoding gradients. Quantitative measures of diffusion are obtained by comparing images with a high b-value (b_{main}) to equivalent images with a lower, typically minimal b-value (b_{ref}). Tensor information is derived from images with the diffusion gradients orientated in ≥6 directions. The tensor is used to calculate mean diffusivity (MD), fractional anisotropy (FA) (15) and helical angle (HA) (9, 16) maps in the left ventricle (6, 7, 11, 17, 18). Published *in-vivo* cDTI studies have typically used b_{main} around 350 s mm^{-2} (b_{ref} has been quoted in few previous studies (19, 20, 21)) with 6 diffusion directions. In reality, signal loss is caused by any intra-voxel incoherent motion and, therefore, contains contributions from both diffusion and microvascular perfusion (22, 23, 24). This has been studied in neurological applications (25, 26, 27), extensively in abdominal diffusion-weighted (i.e. without calculation of a full diffusion tensor) imaging (27, 28, 29) but there is limited work in the heart (24, 30, 31). Callot et al. (24) performed *in-vivo* diffusion-weighted imaging of dog hearts with and without infusion of a vasodilator. The results demonstrated that a two-component model (diffusion + microvascular perfusion) was a good fit to the data; that the component of the model related to perfusion increased after vasodilation; and that the signal loss from both components combined was reduced post-mortem. Using *in-vivo* diffusion-weighted imaging of the human heart Delattre et al. (31) similarly found that a two-component model was a good fit to the data in the heart and liver. However, the effect of microvascular perfusion on tensor parameters derived from *in-vivo* cDTI has, as yet, not been quantified.

In this study we consider how the diffusion weighting, both b_{main} and b_{ref}, influences the measured values of MD, FA and HA in the myocardium of healthy subjects and work towards determining an optimal pair of b-values. This

includes an investigation of the effects of the directionality of the diffusion weighting in b_{ref}.

Methods

Imaging sequence

All imaging was performed using a Skyra 3T MRI scanner (Siemens AG, Erlangen, Germany) with maximum gradient strength 43mTm^{-1} and maximum slew rate 180Tm^{-1}s^{-1} per axis. While other cDTI techniques exist (1, 4, 8, 10, 14, 31), the stimulated-echo acquisition mode (STEAM) echo-planar imaging (EPI) technique with monopolar diffusion encoding is a robust method (6, 7, 9, 18) and was performed in this work during a breath hold using the sequence shown schematically in figure 1 (7, 9). The EPI readout was shortened by using parallel imaging and zonal excitation in the phase encode direction (32). Each stimulated echo was formed over 2 cardiac cycles and each breath hold spanned 18 cardiac cycles. One stimulated echo was used for the EPI phase correction lines, the GRAPPA reference lines, the reference image and for each of the six diffusion encoded images. Diffusion encoding was achieved by using gradients of amplitude (G_d) described in the scanner frame of reference ($\hat{x}, \hat{y}, \hat{z}$) by $G_d\hat{x} \pm G_d\hat{z}$, $G_d\hat{y} \pm G_d\hat{z}$ and $G_d\hat{y} \pm G_d\hat{x}$. Spoiler gradients ($G_{sp}$) are used in the reference acquisitions to spoil the gradient echo from the third RF pulse of the stimulated echo. Although smaller than G_d, the diffusion weighting (b_{ref}) that G_{sp} imparts may be substantial (19). In this work G_{sp} were applied in the imaging frame of reference ($(\hat{m}, \hat{p}, \hat{s})$ spoiler gradient $=G_{sp}\hat{m} + G_{sp}\hat{p} + G_{sp}\hat{s}$) imparting a diffusion weighting of b_{ref}=15 s mm^{-2} to the reference acquisition (subsequently referred to as b_{ref15}). The b-values were calculated (33) using software written in MATLAB (The Mathworks, Natick MA) and the output of the sequence simulator.

The echo-time (TE) was 24ms to enable the maximum prescribed b=950 s mm^{-2} used here (quoted, as all other "prescribed" b-values in this work, for an R-R interval of 1000ms). At this maximum b-value G_d =35mT m^{-1} per axis, ramp time 660μs and flat-top time 1680μs. Lower b-values were achieved by reducing G_d, while maintaining the timing parameters. Other parameters were similar to

those described previously (6, 7): repetition time 2 cardiac cycles; fat suppression; field of view 360 x 135mm^2; slice thickness 8mm; acquired resolution 2.8 x 2.8mm^2; reconstructed resolution 1.4 x 1.4mm^2; GRAPPA factor 2; echo-train length 24 and echo-train duration 13ms.

Data acquisition

Ten healthy subjects (7 male, age 23 – 57) were recruited in accordance with local ethical approval. A short-axis slice in the mid left ventricle was planned from a standard set of balanced steady-state free precession localisers. cDTI was performed in this plane using the sequence described above, triggered to the end-systolic pause ($T_{trigger}$ in figure 1). To determine a suitable range of b_{main} to use in the study one subject was imaged over three sessions with 19 prescribed b-values from 50 to 3000 s mm^{-2}. TE was increased where necessary but other parameters were constant. All subjects were then imaged with 8 averages for prescribed b-values of 50, 150, 350, 550, 750 and 950 s mm^{-2} in a random order to avoid fatigue bias.

Processing

The cDTI data were processed using in-house MATLAB software. All frames were examined visually to identify and reject frames corrupted by motion. A rapid multi-resolution rigid-registration algorithm (34) was used to register all images acquired in the same subject. The diffusion tensor was calculated at every pixel using the linear least squares "B-matrix approach" described in (35). As the mixing time is one cardiac cycle, the actual b-value varies with heart rate. In this work, the images used in the tensor calculation were not averaged so that the dependence of the b-value on heart rate could be accounted for in the B-matrix based on the image time stamps.

Testing the mono-exponential model of diffusion

Typically in DTI, the diffusing water is assumed to be free, which results in a mono-exponential decay of the signal with diffusion weighting:

$$S = S_0 \exp(-b.D) \qquad (1)$$

where S is the measured signal, S_0 is the signal without diffusion weighting, D is the diffusivity along the diffusion encoded direction and b is the magnitude of the diffusion weighting. Including a second, diffusion like, component, which is often performed to account for microvascular perfusion (23, 24, 31), produces a bi-exponential model:

$$S = S_0 \cdot [A\ exp(-b.D_1) + (1 - A)\ exp(-b.D_2)\ ] \quad (2)$$

where D_1 is the diffusion coefficient in the high b-value regime, D_2 describes the diffusion like signal loss at low b-values and A describes the relative contribution of each term.

The relationship between b-value and signal loss was investigated. Trace diffusion-weighted images (8) were calculated for each subject and each b-value. A region of interest (ROI) was defined to cover the left ventricular myocardium in each subject, excluding the papillary muscles. The ratio of the mean trace diffusion-weighted signal and b_{ref15} signal in the ROI was plotted with the corresponding heart rate corrected b-value. The mono and bi-exponential models described in equations 1 and 2 were fitted to this data using the Levenberg-Marquardt algorithm in the MATLAB curve fitting toolbox with the bilinear option for robustness and starting points of A=1.0, D_1=D_2=1.0x10^{-3} mm^2s^{-1}.

Comparison of combinations of b_{main} and b_{ref} values

To assess the effect of b_{main}, the MD, FA and HA parameter maps were calculated for each subject using each of the 6 acquired b-values (prescribed as 50 – 950 s mm^{-2}) as b_{main} together with the b_{ref15} images.

To determine the effect of the diffusion weighting of the reference image on the parameter maps, diffusion-weighted images were used as a reference (b_{refD} images). To determine the best way to acquire diffusion weighted reference data, 3 methods of defining the reference data were used:

Method 1 – ALL: All averages and directions were used for the reference data. This theoretically represents the best reference data, but in practice, means doubling the acquisition duration as 6 directions with 8 averages are used for both the b_{main} images and the b_{refD} images.

Method 2 – 1DIR: All averages of the first diffusion direction were used as reference images. This most closely approximates the diffusion weighting of the spoiler gradients used in the b_{ref15} images, although in general, the direction of the diffusion weighting of the b_{ref15} images is not parallel to any of the diffusion encoding directions. This scheme could be implemented without increasing the acquisition duration beyond the previously described protocol (7). The first direction was chosen here arbitrarily and this process also was repeated using the second (perpendicular to the first) and third (greatest sum of squares difference from the first direction) directions to test any dependence on direction.

Method 3 – 1AVE: The first average of all directions was used as reference data. Although with less signal to noise ratio (SNR) than in method 1 (ALL), this scheme could be implemented without increasing the acquisition duration beyond the previously described protocol (7).

For each subject and using each b-value as b_{main}, diffusion tensors and MD, FA and HA parameter maps were calculated using all possible b_{refD} with all three methods described above. Mean FA and MD in the left ventricle ROI was calculated for each case. HA varies approximately linearly from endo- to epicardium so the mean HA gradient and mean coefficient of determination (R^2) from a linear regression of HA versus transmural depth (20, 21) was calculated to provide an indication of the changes in HA with b_{main} and b_{ref}. The number of negative eigenvalues in the calculated diffusion tensor within the ROI was also recorded. These values violate the assumption that the diffusion tensor is positive definite and they are, therefore, unphysical so are used as an indicator of

poor quality data where, for instance, the difference in signal between the voxels in the main and reference data was insufficient.

Measures of SNR

The SNR was calculated from the trace diffusion-weighted images using the method described in Nielles-Vallespin et al. (7, 36), where SNR was defined as the ratio of the mean signal to the standard deviation between averages in each pixel. The mean SNR in the left ventricle and in each of 4 equal angle segments (septal, anterior, lateral and inferior) was calculated. In addition, minimum signal to noise floor ratio (MSNFR) was defined as the ratio of the minimum value (over the six directions) from the diffusion images after averaging all images with the same diffusion encoding, to the mean signal value in a ROI drawn in the blood pool in the left ventricle. The mean MSNFR was calculated in each of the 4 segments to indicate the proximity of the diffusion-weighted signal to the noise floor.

Results

cDTI was successfully performed in all subjects and no breath holds were repeated due to poor image quality. The mean number of rejected frames per acquisition was 3.1±7.5% and the number of rejected frames did not correlate significantly with prescribed b-values (R^2=0.0025, p=0.81). The median acquisition duration for the cDTI data acquisition was 32 minutes (range 28 – 40 minutes). The median for all 10 subjects of the average RR interval was 1.055 s with a range of 0.83 – 1.22 s corresponding to b-values from 623 – 915 s mm^{-2} for a prescribed b-value of 750 s mm^{-2} (which, in combination with b_{ref}=150 s mm^{-2}, we later find to be optimal). The median within-subject standard deviation of the RR interval was 0.05 (range 0.03 – 0.06 s), suggesting that at a prescribed b-value of 750 s mm^{-2} and a mean RR interval of 1s the b-value typically varied within a subject from 675 to 825 s mm^{-2} (-2 standard deviations to +2 standard deviations). Figure 2 shows example images at each of the prescribed b-values before and after averaging in one typical subject. Artifacts caused by insufficient spoiling of the gradient echo pathways were observed in

some b_{ref15} images (Figure 2a arrow). These artifacts were not present in any of the other diffusion-weighted images, due to the higher b-values and more effective spoiling in these images.

Plots of MD, FA, SNR and MSNFR versus prescribed b_{main} up to 3000 s mm^{-2} (with b_{ref15}) for the pilot subject are provided in the supplementary material (S1). MD initially fell rapidly until b_{main}≈250 s mm^{-2} and then more slowly. FA reduces with increasing b_{main}, with a more rapid reduction beginning between prescribed b_{main}=750 s mm^{-2} and b_{main}=950 s mm^{-2}. Visual analysis suggests that signal in some areas of the myocardium reaches the noise level at around prescribed b_{main}=950 s mm^{-2} and the MSNFR is less than 2 at this point. Based on these results, prescribed b-values from 50 to 950 s mm^{-2} were chosen to image the 10 volunteers.

Figure 3 shows maps of MD, FA and HA from one typical subject with all b_{main} values and b_{ref15} reference images. The parameter maps appear more consistent between b_{main} values as b_{main} increases.

Figure 4 shows a plot of the mean myocardial signal intensity in the trace diffusion-weighted images plotted against the heart rate corrected b-value. The fit of equations 1 and 2 to the data after excluding data at b-values >1000 s mm^{-2} to avoid the noise floor is also shown. The bi-exponential model (equation 2) demonstrates better agreement with the data than the mono-exponential model, R^2=0.994 vs. R^2=0.987 respectively. The fitted parameters for the bi-exponential model were D_1 =0.86 x 10^{-3} mm^2 s^{-1} (95% confidence interval (C.I.) =0.83–0.90 x 10^{-3} mm^2 s^{-1}), D_2 =17 x 10^{-3} mm^2 s^{-1} (C.I. =5.6 – 29 x 10^{-3} mm^2 s^{-1}) and A=0.94 (C.I. =0.92 – 0.96). The mono-exponential model over-estimates the diffusivity when compared to the bi-exponential model as D =0.99 x 10^{-3}mm^{2}s^{-1} (C.I. 0.95 – 1.00 x 10^{-3}mm^{2}s^{-1}).

Diffusion tensors and the parameter maps were calculated for every subject with all b_{main}/b_{refD} combinations using all three methods. Figure 5 shows the mean MD, FA, HA gradient, R^2 from the transmural linear regression of HA and

percentage of negative eigenvalues plotted against Δb (where Δb is the difference between the prescribed b_{main} and b_{ref}). For clarity, the results obtained using b_{ref15} are shown for each b_{main} value and the full set of results using all possible b_{refD} values is only provided for b_{main}=750 s mm^{-2} and the 1AVE method (the complete set of results is provided in supplementary material, figure S2).

When the b_{ref15} images are used as a reference, the MD initially falls rapidly with Δb and then more gradually when Δb>150 s mm^{-2} (figure 5.a). With increasing b_{refD} MD falls slowly. There is little difference in MD values between the ALL, 1DIR and 1AVE methods (see supplementary material, figure S2. a-c).

There is a significant linear trend for decreasing FA with increasing Δb using ALL (R^2=0.95, p<0.001, FA=0.49 – 0.00013 Δb), 1DIR (R^2=0.93, p<0.001, FA=0.50 – 0.00014 Δb) and 1AVE (R^2=0.94, p<0.001, FA=0.49 – 0.00013 Δb) (see figure 5.b and supplementary material, figure S2, d-f).

The percentage of negative eigenvalues is high (up to 23%) for small values of Δb (≤ 200 s mm^{-2}, see figure 5.c), suggesting that the data is unreliable in this regime. At low Δb the percentage of negative eigenvalues increases with increasing b_{refD}; more so when 1DIR or 1AVE is used (see supplementary material figure S2, g-i). However, when Δb > 200 s mm^{-2}, the maximum mean number of negative eigenvalues was 0.8%.

When Δb ≤ 200 s mm^{-2}, there is a small increase in HA gradient for some combinations of b_{main}, b_{ref} and reference method (see supplementary material figure S2, m-o). The R^2 value from the linear regression of transmural HA change primarily depends on b_{main} and is low at low b_{main}, then plateaus around b_{main}=550 s mm^{-2}. When the 1AVE or 1DIR methods are used there is a small drop in R^2 value with increasing b_{ref} value (see supplementary material, figure S2, j-l).

While there is a greater proportion of negative eigenvalues at small Δb when using 1AVE or 1DIR compared to using ALL, differences in HA gradient, FA and

MD between the methods are small. As the ALL method is time consuming and appears to offer little benefit, either of 1DIR or 1AVE should be considered optimal.

Tables 1 and 2 provide mean MD and FA values calculated from all pairs of prescribed b_{main} and b_{refD} using the 1AVE method of calculating b_{refD}. MD is closest to D_1 when prescribed b_{main}=950 s mm^{-2} and b_{refD}=50 s mm^{-2} (MD=0.859±0.053 s mm^{-2}) and next closest when b_{main}=750 s mm^{-2} and b_{refD}=150 s mm^{-2} (MD=0.870±0.063 s mm^{-2}).

SNR and MSNFR were highest in the septal segment and lowest in the lateral segment. Plots of mean SNR and MSNFR in the septal and lateral segments with b-value are provided in the supplementary material (figure S3). As expected SNR and MSNFR decrease with increasing b-value. In the lateral wall the MSNFR at prescribed b=950 s mm^{-2} is 1.47±0.28, which is 1.7 standard deviations away from the noise floor and it might be expected that the signal in some subjects may lie within the noise floor. At prescribed b=750 s mm^{-2}, MSNFR is 1.74±0.37, which is 2.0 standard deviations from the noise floor and in the large majority of healthy subjects the signal avoids noise floor effects.

Figure 6 shows example parameter maps (MD, FA and HA) in one subject when prescribed b_{main}=750 s mm^{-2} and the prescribed b_{ref} is increased from 15 to 550 s mm^{-2} using the 1AVE (part i) and 1DIR (part ii) methods of calculating b_{refD}. There is little difference between the parameter maps produced using 1AVE and 1DIR, except a slightly greater visible increase in noise in the FA and MD maps as b_{refD} is increased using 1AVE.

When the processing was repeated using the 1DIR method of calculating the b_{refD} images using the second diffusion encoding direction as a reference, there was an average difference in MD of +2.3 ± 2.7% and FA of -2.1±2.6% (direction 1 – direction 2) at b_{main}=750 s mm^{-2} and b_{refD}=150 s mm^{-2}. The equivalent results using the third diffusion encoding direction as a reference were a difference in MD of +1.5±3.5% and in FA of -1.3±3.1% (direction 1 – direction 3). When

b_{main}=350s mm^{-2} and b_{refD}=150s mm^{-2}, there was an MD difference of +2.9±7.2% and an FA difference of -2.5±5.6% when comparing direction 1 to direction 2. The equivalent results comparing direction 1 to direction 3 were an MD difference of +3.4±9.2% and an FA difference of -2.8±7.0%.

Figure 7 shows FA maps, MD maps and superquadric glyphs representing the full measured diffusion tensor in each pixel for one subject with prescribed b_{main}=350 s mm^{-2} and b_{refD}=150 s mm^{-2}, using the 1DIR method (figure 7a, c, e and f) and with prescribed b_{main}=750 s mm^{-2} and b_{refD}=150 s mm^{-2} using the 1AVE method (figure 7b, d, g and h). Table 3 compares values for MD, FA, HA gradient and R^2 for prescribed b_{main}=350 and 750 s mm^{-2} when b_{ref15} and b_{refD}=150 s mm^{-2} (all three methods) are used as a reference. These b-values were chosen to most closely match those in previous work from both our group (6, 7, 19, 21) and others (9, 11, 12, 20), compared with the values chosen as optimal in this work.

Discussion

In this work we have described developments, which go some way towards addressing two of the difficulties faced in *in-vivo* cDTI: the intrinsically low SNR of the technique and the contribution of other intra-voxel incoherent motions to the measured diffusion. We have demonstrated the dependence of the measured myocardial diffusivity on b_{main}. This is partly caused by a deviation of the signal intensity versus b-value relationship from the mono-exponential model shown in equation 1. A bi-exponential model fits the data well. At low b-values the signal loss is a combination of the diffusion of water molecules (described by D_1) and a second process with a much higher apparent diffusion coefficient (D_2), which, it has been suggested (31), is associated with microvascular perfusion. In this study, using b_{ref}=150 s mm^{-2} was sufficient to reduce the contribution of the D_2 component to 0.5% of the remaining signal, making MD less dependent on the b_{main}. One limitation of this analysis was that it did not consider any directionality of the two components. Previous work (24, 30) has suggested that the fast (or D_2) component is predominantly aligned with the myocyte orientation, but others (31) have assumed D_2 to be isotropic.

Our results demonstrate that when a similar number of b_{ref} images are used, mean values of FA, MD and HA gradient are similar whether the reference images have diffusion encoding in a single direction (1DIR) or the direction is rotated (1AVE). However, we did demonstrate within-subjects differences in FA and MD depending on which diffusion encoding direction was used as a reference with the 1DIR technique. And while it was not investigated as part of this work, it would seem reasonable to acquire reference data with diffusion encoded in several directions to avoid any directional bias in D_2 (24). Parameter maps are improved using the ALL method, but it is not clear from this work whether time would be better used to acquire more data at b_{ref} or b_{main}. In future studies b_{refD} images may be acquired instead of or in addition to the existing b_{ref15} images; acquiring both may allow an estimation of D_2 which could be physiologically interesting.

Prescribed b_{main}, particularly for low SNR techniques such as STEAM, should be as high as possible to maximise the signal intensity differences between the main and reference data, and hence, increase the SNR of the derived tensors. With increasing b_{ref} derived parameters become more variable and at low Δb values, there are more negative eigenvalues. The minimum value of b_{ref} required to suppress the signal from microvascular perfusion should therefore, be used. The longer diffusion gradients required for higher b-values increase TE slightly, but the disadvantages of this should be outweighed by the improvements in the parameter maps. At sufficiently high b-values the signal approaches the noise floor and the derived parameters will be artifactually affected (37). The signal is closer to the noise floor in the lateral wall than in the septal wall, but MSNFR (and SNR) is more variable in the septal wall (see the standard deviations in supplementary figure S2). This is due to the combination of the proximity of the septal wall to the anterior surface coil, the rapid change in coil sensitivity in this region and the subject specific cardiac geometry. We calculated parameter maps using prescribed b_{main} values up to 950 s mm^{-2}, without noticing detrimental effects. However, limiting prescribed b_{main} to 750 s mm^{-2} maintained MSNFR at 2 standard deviations above the noise floor in healthy subjects. In patients the

prescribed b_{main} may need to be reduced below 750 s mm^{-2} as patients often have a higher body mass index and poorer breath-hold performance, both of which reduce SNR.

For the protocol used in this study, we selected a combination of b_{main} = 750 s mm^{-2} with b_{refD} = 150 s mm^{-2} as optimal. This was based on reducing the contribution of D_2 to less than 1% of the remaining signal, avoiding severe noise floor effects at high b-values, matching the mean MD value to the D_1 value obtained and maximising the linearity of the transmural HA progression (R^2). It is possible that a different combination would be optimal for FA, which reduced linearly with Δb. Improvements in the appearance of FA maps were observed with increasing Δb but without a gold standard for myocardial FA, this remains a limitation.

Until now there has been little consideration of the optimal b-values for *in-vivo* cDTI. Previous work in neuro-imaging has suggested that Δb should be approximately 1.11/diffusivity (38) (ignoring T2), suggesting that Δb should, be larger than the value of 600 s mm^{-2} (b_{main}=750 and b_{refD}=150 s mm^{-2}) selected here as optimal. While future improvements (39) may permit larger Δb values, a detailed assessment, including simulations of the effects of noise should be performed first.

The FA and MD obtained here using prescribed b_{main}=350 s mm^{-2} and b_{refD}=150 s mm^{-2} calculated using the 1DIR method are within 1 standard deviation of those obtained by Nielles-Vallespin et al. (prescribed b_{main}=350 s mm^{-2}) after the correction for b_{ref} (prescribed at 135 s mm^{-2}) was applied (7, 19) (FA=0.471±0.041 vs. 0.46±0.04 and MD=0.987±0.082 x 10^{-3} mm^2 s^{-1} vs. 1.14±0.15 x 10^{-3} mm^2 s^{-1}). Wu et al. (12) found MD=0.64 ± 0.03 x 10^{-3} mm^2 s^{-1} in healthy subjects, imaged at the sweet spot to avoid strain effects, using monopolar STEAM EPI (b_{main}=300 s mm^{-2}). We found higher MD values (MD=1.049±0.047 x 10^{-3} mm^2 s^{-1} using prescribed b_{main}=350 s mm^{-2} and b_{ref15}), but acquired at peak systole, where strain affects measurements, but motion is less problematic. Using similar sequences (b_{main}=350 s mm^{-2} and b_{ref}=15-20 s

mm^{-2}) also acquired in peak systole, Lau et al. (20) and Tunnicliffe et al. (21) obtained closer values of MD=1.19±0.10 x 10^{-3} mm^2 s^{-1} and MD=1.06±0.06/1.13±0.13 x 10^{-3} mm^2 s^{-1} (two-centre comparison (21)) respectively. Using diffusion-weighted imaging, Rapacchi et al. (8) found MD=7.1 x 10^{-3} mm^2 s^{-1} using a spin-echo EPI sequence with b=0, 50 and 100 s mm^{-2}, which is greater than we found (MD=1.90±0.46 x 10^{-3} mm^2 s^{-1} using prescribed b_{main}=50 s mm^{-2} and b_{ref15}). At low b_{main} the measured MD is elevated due to the inclusion of microvascular perfusion and the high ratio of noise to signal difference between the main and reference images. The same group also fitted a bi-exponential model to diffusion-weighted data acquired with b-values from b=0 to b=550 s mm^{-2} (31). They found values equivalent to our D_1, D_2 and A of D_1=2.44±0.99 x 10^{-3} mm^2 s^{-1}, D_2=76.5 x 10^{-3} mm^2 s^{-1} and A=0.792±0.057. Using a larger range but fewer b-values, we found a smaller proportion of microvascular perfusion (A=0.94) and lower values for both D_1=0.86 x 10^{-3} mm^2 s^{-1} and D_2=17 x 10^{-3} mm^2 s^{-1}. One key difference with our work is the mixing time, which is ~10ms for the spin-echo sequence and ~1s for the monopolar STEAM sequence. *Ex-vivo* work has demonstrated time dependent diffusivity in myocardial tissue (5), however it is unclear how this would translate to *in-vivo* imaging. Work in *in-vivo* canine myocardium using a monopolar STEAM EPI sequence (14 b-values, 0-600 s mm^{-2}, mixing time 1 cardiac cycle) has found values equivalent to D_1=1.26±0.10 x 10^{-3} mm^2 s^{-1} and D_2=14.13±2.56 x 10^{-3} mm^2 s^{-1} (24).

We have demonstrated a dependence of FA on the b-values. We obtained mean FA values from 0.372 (prescribed b_{main}=950 s mm^{-2} and b_{ref15}) to 0.495 (prescribed b_{main}=150 and b_{ref15}). In healthy volunteers Wu et al. (12), measured FA=0.34±0.02 at b_{main}=300 s mm^{-2}, whereas Tseng et al. (11) quote higher values of FA=0.72 and 0.78 in the free wall and septum respectively (b_{main}=400 s mm^{-2}). However, FA might be elevated at the higher spatial resolution used by Tseng et al. (3x3x3mm^3) (11). Using a protocol similar to that used here, similar values to our result of FA=0.445±0.042 (using b_{ref15} and b_{main}=350 s mm^{-2}) were found by Lau et al. (20) (FA=0.44±0.05) and Tunnicliffe et al. (21) (FA=0.41±0.05 and 0.40±0.07 at two sites).

The values of HA gradient obtained by Tunnicliffe et al. (21) were similar to those obtained here (8.7±1.4 and 9.0±1.4 ^{o} mm^{-1} at two different sites vs. 9.3±1.1 ^{o} mm^{-1} here using b_{main}=350 s mm^{-2} and b_{ref15}), but Lau et al. (20), found a lower value of 4.5 ±1.5 ^{o} mm^{-1}. HA gradient appears to change little with b-values but using the coefficient of determination of the linear fit (R^2) appears to be an indicator of data quality and demonstrated that HA is most linear when $b_{main} \geq$ 550 s mm^{-2}.

The results we have presented here apply to the monopolar STEAM technique and the optimal parameters will vary with subject and protocol. The dependence of the b-value on the heart rate means that it is important that the dependence of measured diffusion parameters on the b-values is minimized to enable between-subjects comparisons. It is also possible parameters could vary with heart rate due to a mixing time dependence of the measured diffusion which is typical in biological tissues (40). However, from *ex-vivo* work, we expect the changes to be small for typical variations in heart rate (5). While we did not eliminate the dependence of FA and MD on b-values, work in the brain (41, 42, 43) has demonstrated that a mono-exponential model is insufficient at higher b_{main} values, due to the complex structure of biological tissues. In fact previous work in *ex-vivo* myocardium, has shown reductions in FA and MD (13) and deviation from mono-exponential behavior in isolated beating hearts (30) at high b_{main} values. As described by Jones et al. (37), there is a signal bias effect before we reach the noise floor which would account for some of the changes we observed in MD and FA (37). Also, we did not account for strain (9, 44, 45), but it should have similar effects on any intravoxel incoherent motion and we believe our findings still apply.

In conclusion, we have demonstrated how *in-vivo* cDTI may be improved by using optimal b-values. We have demonstrated the dependence of MD, FA and transmural HA linearity on diffusion weighting and shown that at low b-values the signal loss in *in-vivo* cDTI is dominated by a second process with a high diffusion coefficient. We believe this additional process to be microvascular perfusion and its contribution to the measured diffusivity can be avoided by

using diffusion-weighted reference images. Also, using increased diffusion weighting in the main diffusion-weighted images improves the MD, FA and HA maps, as long as the diffusion-weighted signal remains sufficiently far from the noise floor. While the noise floor depends on many parameters, a combination of prescribed b_{main}=750 s mm^{-2} and b_{ref}=150 s mm^{-2} was optimal for the protocol used here and is recommended as a starting point for future developments. The improvements in parameter maps provided by using these optimal b-values might enable detection of the seemingly small changes caused by disease and contribute to advances in the understanding of cardiac microstructure.

Acknowledgements

This work was performed at the National Institute of Health Research funded Cardiovascular Biomedical Research Unit at the Royal Brompton Hospital, London, UK.

References

1. Dou J, Reese TG, Tseng WI, Wedeen VJ. Cardiac diffusion MRI without motion effects. Magn Reson Med 2002; 48: 105-14.

2. Dou J, Tseng WI, Reese TG, Wedeen VJ. Combined diffusion and strain MRI reveals structure and function of human myocardial laminar sheets in vivo. Magn Reson Med 2003; 50: 107-13.

3. Edelman RR, Gaa J, Wedeen VJ, Loh E, Hare JM, Prasad P, Li W. In vivo measurement of water diffusion in the human heart. Magn Reson Med 1994; 32: 423-8.

4. Gamper U, Boesiger P, Kozerke S. Diffusion imaging of the in vivo heart using spin echoes--considerations on bulk motion sensitivity. Magn Reson Med 2007; 57: 331-7.

5. Kim S, Chi-Fishman G, Barnett AS, Pierpaoli C. Dependence on diffusion time of apparent diffusion tensor of ex vivo calf tongue and heart. Magn Reson Med 2005; 54: 1387-96.

6. McGill L, Ismail TF, Nielles-Vallespin S, Ferreira P, Scott AD, Roughton M, Kilner PJ, Ho SY, McCarthy KP, Gatehouse PD, others. Reproducibility of in-vivo

diffusion tensor cardiovascular magnetic resonance in hypertrophic cardiomyopathy. J Cardiovasc Magn Reson 2012; 14: 86.
7. Nielles-Vallespin S, Mekkaoui C, Gatehouse P, Reese TG, Keegan J, Ferreira PF, Collins S, Speier P, Feiweier T, de Silva R, Jackowski MP, Pennell DJ, Sosnovik DE, Firmin D. In vivo diffusion tensor MRI of the human heart: reproducibility of breath-hold and navigator-based approaches. Magn Reson Med 2013; 70: 454-65.
8. Rapacchi S, Wen H, Viallon M, Grenier D, Kellman P, Croisille P, Pai VM. Low b-value diffusion-weighted cardiac magnetic resonance imaging: initial results in humans using an optimal time-window imaging approach. Invest Radiol 2011; 46: 751-8.
9. Reese TG, Weisskoff RM, Smith RN, Rosen BR, Dinsmore RE, Wedeen VJ. Imaging myocardial fiber architecture in vivo with magnetic resonance. Magn Reson Med 1995; 34: 786-91.
10. Toussaint N, Stoeck CT, Schaeffter T, Kozerke S, Sermesant M, Batchelor PG. In vivo human cardiac fibre architecture estimation using shape-based diffusion tensor processing. Med Image Anal 2013; 17: 1243-55.
11. Tseng WI, Dou J, Reese TG, Wedeen VJ. Imaging myocardial fiber disarray and intramural strain hypokinesis in hypertrophic cardiomyopathy with MRI. J Magn Reson Imaging 2006; 23: 1-8.
12. Wu M, Su MM, Huang Y, Chiou K, Yang P, Pan H, Reese TG, Wedeen VJ, Tseng WI. Sequential changes of myocardial microstructure in patients postmyocardial infarction by diffusion-tensor cardiac MR: correlation with left ventricular structure and function. Circ Cardiovasc Imaging 2009; 2: 32-40, 6 p following 40.
13. Wu Y, Zou C, Liu W, Liao W, Yang W, Porter DA, Liu X, Wu EX. Effect of B-value in revealing postinfarct myocardial microstructural remodeling using MR diffusion tensor imaging. Magn Reson Imaging 2013; 31: 847-56.
14. Nguyen C, Fan Z, Sharif B, He Y, Dharmakumar R, Berman DS, Li D. In vivo three-dimensional high resolution cardiac diffusion-weighted MRI: A motion compensated diffusion-prepared balanced steady-state free precession approach. Magn Reson Med 2013. doi: 10.1002/mrm.25038.
15. Basser PJ, Pierpaoli C. Microstructural and Physiological Features of

Tissues Elucidated by Quantitative-Diffusion-Tensor MRI. Journal of Magnetic Resonance, Series B 1996; 111: 209-219.
16. Scollan DF, Holmes A, Winslow R, Forder J. Histological validation of myocardial microstructure obtained from diffusion tensor magnetic resonance imaging. Am J Physiol 1998; 275: H2308-18.
17. Tseng WI, Wedeen VJ, Reese TG, Smith RN, Halpern EF. Diffusion tensor MRI of myocardial fibers and sheets: correspondence with visible cut-face texture. J Magn Reson Imaging 2003; 17: 31-42.
18. Wu M, Tseng WI, Su MM, Liu C, Chiou K, Wedeen VJ, Reese TG, Yang C. Diffusion tensor magnetic resonance imaging mapping the fiber architecture remodeling in human myocardium after infarction: correlation with viability and wall motion. Circulation 2006; 114: 1036-45.
19. Nielles-Vallespin S, Mekkaoui C, Gatehouse P, Reese TG, Keegan J, Ferreira PF, Collins S, Speier P, Feiweier T, de Silva R, Jackowski MP, Pennell DJ, Sosnovik DE, Firmin D. Erratum: In vivo diffusion tensor MRI of the human heart: Reproducibility of breath-hold and navigator based approaches. Magn Reson Med 2013;70:454-465.. Magnetic Resonance in Medicine 2014. doi: 10.1002/mrm.25237.
20. Lau AZ, Tunnicliffe EM, Frost R, Koopmans PJ, Tyler DJ, Robson MD. Accelerated human cardiac diffusion tensor imaging using simultaneous multislice imaging. Magn Reson Med 2014. doi: 10.1002/mrm.25200.
21. Tunnicliffe EM, Scott AD, Ferreira P, Ariga R, McGill L, Nielles-Vallespin S, Neubauer S, Pennell DJ, Robson MD, Firmin DN. Intercentre reproducibility of cardiac apparent diffusion coefficient and fractional anisotropy in healthy volunteers. J Cardiovasc Magn Reson 2014; 16: 31.
22. Le Bihan D, Breton E, Lallemand D, Grenier P, Cabanis E, Laval-Jeantet M. MR imaging of intravoxel incoherent motions: application to diffusion and perfusion in neurologic disorders. Radiology 1986; 161: 401-7.
23. Le Bihan D, Breton E, Lallemand D, Aubin ML, Vignaud J, Laval-Jeantet M. Separation of diffusion and perfusion in intravoxel incoherent motion MR imaging. Radiology 1988; 168: 497-505.
24. Callot V, Bennett E, Decking UKM, Balaban RS, Wen H. In vivo study of microcirculation in canine myocardium using the IVIM method. Magn Reson Med

2003; 50: 531-40.
25. Maki JH, MacFall JR, Johnson GA. The use of gradient flow compensation to separate diffusion and microcirculatory flow in MRI. Magn Reson Med 1991; 17: 95-107.
26. Mulkern RV, Haker SJ, Maier SE. On high b diffusion imaging in the human brain: ruminations and experimental insights. Magn Reson Imaging 2009; 27: 1151-62.
27. Tachibana Y, Aida N, Niwa T, Nozawa K, Kusagiri K, Mori K, Endo K, Obata T, Inoue T. Analysis of multiple B-value diffusion-weighted imaging in pediatric acute encephalopathy. PLoS One 2013; 8: e63869.
28. Yamada I, Aung W, Himeno Y, Nakagawa T, Shibuya H. Diffusion coefficients in abdominal organs and hepatic lesions: evaluation with intravoxel incoherent motion echo-planar MR imaging. Radiology 1999; 210: 617-23.
29. Koh D, Thoeny HC. Diffusion-Weighted MR Imaging: Applications in the Body. Springer 2010.
30. Hsu EW, Buckley DL, Bui JD, Blackband SJ, Forder JR. Two-component diffusion tensor MRI of isolated perfused hearts. Magn Reson Med 2001; 45: 1039-45.
31. Delattre BMA, Viallon M, Wei H, Zhu YM, Feiweier T, Pai VM, Wen H, Croisille P. In vivo cardiac diffusion-weighted magnetic resonance imaging: quantification of normal perfusion and diffusion coefficients with intravoxel incoherent motion imaging. Invest Radiol 2012; 47: 662-70.
32. Feinberg DA, Turner R, Jakab PD, Kienlin MV. Echo-planar imaging with asymmetric gradient modulation and inner-volume excitation. Magn Reson Med 1990; 13: 162-169.
33. Stejskal E, Tanner J. Spin diffusion measurements: Spin echoes in the presence of a time-dependent field gradient. The journal of chemical physics 2004; 42: 288--292.
34. Guizar-Sicairos M, Thurman ST, Fienup JR. Efficient subpixel image registration algorithms. Optics letters 2008; 33: 156-158.
35. Kingsley PB. Introduction to diffusion tensor imaging mathematics: Part III. Tensor calculation, noise, simulations, and optimization. Concepts in Magnetic Resonance Part A 2006; 28A: 155--179.

36. Reeder SB, Wintersperger BJ, Dietrich O, Lanz T, Greiser A, Reiser MF, Glazer GM, Schoenberg SO. Practical approaches to the evaluation of signal-to-noise ratio performance with parallel imaging: application with cardiac imaging and a 32-channel cardiac coil. Magn Reson Med 2005; 54: 748-54.
37. Jones DK, Basser PJ. "Squashing peanuts and smashing pumpkins": how noise distorts diffusion-weighted MR data. Magn Reson Med 2004; 52: 979-93.
38. Jones DK, Horsfield MA, Simmons A. Optimal strategies for measuring diffusion in anisotropic systems by magnetic resonance imaging. Magn Reson Med 1999; 42: 515-25.
39. Bammer R, Holdsworth SJ, Veldhuis WB, Skare ST. New methods in diffusion-weighted and diffusion tensor imaging. Magn Reson Imaging Clin N Am 2009; 17: 175-204.
40. Novikov DS, Fieremans E, Jensen JH, Helpern JA. Random walks with barriers. Nature physics 2011; 7: 508--514.
41. Jensen JH, Helpern JA, Ramani A, Lu H, Kaczynski K. Diffusional kurtosis imaging: The quantification of non-gaussian water diffusion by means of magnetic resonance imaging. Magn Reson Med 2005; 53: 1432-1440.
42. Niendorf T, Dijkhuizen RM, Norris DG, van Lookeren Campagne M, Nicolay K. Biexponential diffusion attenuation in various states of brain tissue: implications for diffusion-weighted imaging. Magn Reson Med 1996; 36: 847-57.
43. Norris DG. The effects of microscopic tissue parameters on the diffusion weighted magnetic resonance imaging experiment. NMR Biomed 2001; 14: 77-93.
44. Reese, Wedeen, Weisskoff. Measuring Diffusion in the Presence of Material Strain. J Magn Reson B 1996; 112: 253-8.
45. Tseng WY, Reese TG, Weisskoff RM, Wedeen VJ. Cardiac diffusion tensor MRI in vivo without strain correction. Magn Reson Med 1999; 42: 393-403.

Tables

Table 1: Mean (±SD) of global left ventricular MD using the 1AVE method of calculating the reference images.

b_{ref}	b_{main} 50	b_{main} 150	b_{main} 350	b_{main} 550	b_{main} 750	b_{main} 950
b_{ref15}	1.90 ±0.46	1.21 ±0.17	1.049 ±0.047	0.983 ±0.041	0.930 ±0.037	0.879 ±0.041
50		1.19 ±0.16	1.012 ±0.053	0.954 ±0.055	0.906 ±0.053	0.859 ±0.053
150			0.97 ±0.16	0.914 ±0.092	0.870 ±0.063	0.827 ±0.053
350				0.89 ±0.12	0.826 ±0.075	0.784 ±0.072
550					0.823 ±0.087	0.763 ±0.082
750						0.72 ±0.14

The cells highlighted grey indicate where the calculated MD deviates by 10% or less from the value of D_1 calculated in figure 4. MD values are given in units of $\times 10^{-3}$ mm^2 s^{-1} and b-values are prescribed and in units of s mm^{-2}.

Table 2: Mean (±SD) of global left ventricular FA using the 1AVE method of calculating the reference images.

b_{ref}	b_{main} 50	b_{main} 150	b_{main} 350	b_{main} 550	b_{main} 750	b_{main} 950
b_{ref15}	0.481 ±0.023	0.492 ±0.062	0.445 ±0.042	0.411 ±0.026	0.393 ±0.021	0.372 ±0.029
50		0.491 ±0.045	0.461 ±0.042	0.424 ±0.029	0.404 ±0.023	0.382 ±0.030
150			0.483 ±0.068	0.444 ±0.045	0.419 ±0.036	0.396 ±0.038
350				0.461 ±0.043	0.448 ±0.029	0.420 ±0.027
550					0.453 ±0.042	0.435 ±0.031
750						0.451 ±0.059

b-values are prescribed and are given in units of s mm^{-2}.

Table 3: Comparison of the 3 methods of acquiring reference data

b_{main}	b_{ref}	Ref. method	MD (mean ± SD)	FA (mean ± SD)	HA gradient (mean ± SD)	R^2 (mean ± SD)
350	15	b_{ref15}	1.049±0.047	0.445±0.042	9.3±1.1	0.861±0.067
350	150	ALL	0.960±0.076	0.482±0.032	9.2±1.2	0.870±0.059
350	150	1DIR	0.987±0.082	0.471±0.041	9.4±1.1	0.856±0.063
350	150	1AVE	0.974±0.157	0.483±0.068	9.2±1.1	0.850±0.062
750	15	b_{ref15}	0.930±0.037	0.393±0.021	9.1±1.0	0.908±0.035
750	150	ALL	0.875±0.070	0.418±0.023	9.17±0.97	0.912±0.038
750	150	1DIR	0.883±0.055	0.412±0.023	9.1±1.0	0.909±0.036
750	150	1AVE	0.870±0.064	0.419±0.036	9.0±1.0	0.910±0.032

MD values are quoted in units of x 10^{-3} mm^2 s^{-1}.

HA gradient is quoted in units of ^{o} mm^{-1}.

R^2 is the coefficient of determination for the linear regression of transmural HA progression.

b-values are prescribed and are given in units of s mm^{-2}.

The grey rows highlight the protocol which approximately replicates the method used in McGill et al. (6) and Nielles-Vallespin et al. (7, 19) (prescribed b_{main}=350 s mm^{-2}, 1DIR method b_{refD}=135 s mm^{-2}) compared to the parameters proposed for future studies (prescribed b_{main}=750 s mm^{-2}, 1AVE method b_{refD}=150 s mm^{-2}).

Figures

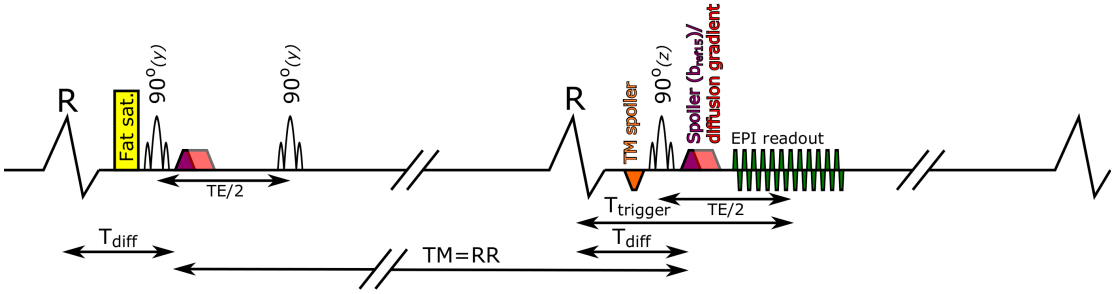

Figure 1: The monopolar STEAM EPI sequence used in this study. TM = mixing time, TE = echo time, $T_{Trigger}$ = trigger time for imaging, T_{diff} = time the diffusion gradients are applied.

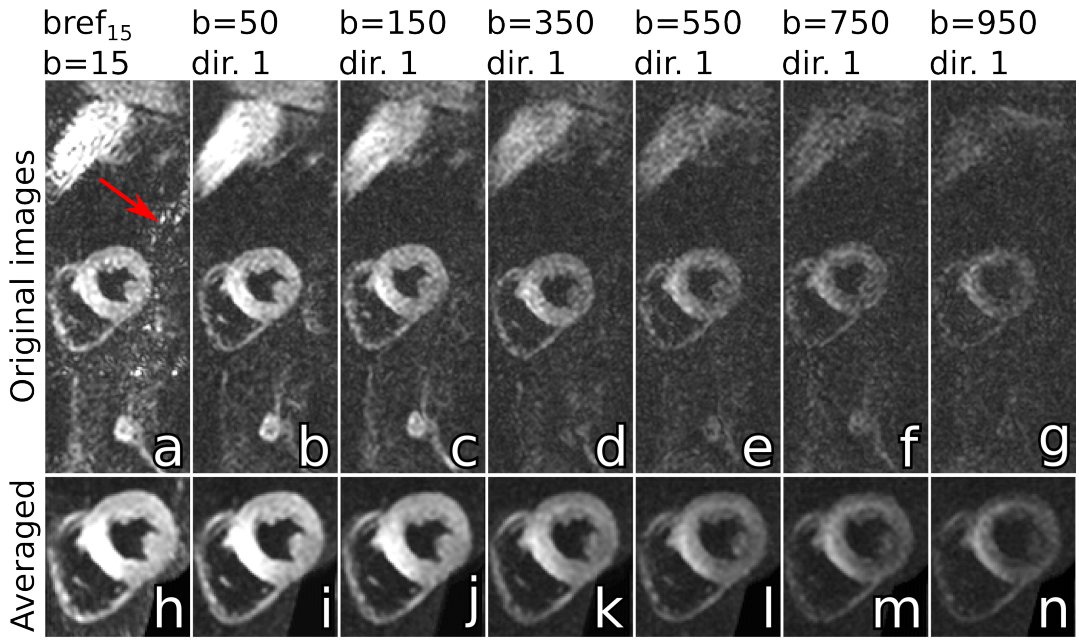

Figure 2: Example diffusion encoded images with increasing diffusion weighting, both with one average (a – g) and after motion correction and averaging (h – n). Artifact is observed in the b_{ref15} images before averaging (arrow), thought to be due to incomplete spoiling of gradient and spin echoes at low b-values. b-values are prescribed (not heart rate corrected) in units of s mm^{-2}.

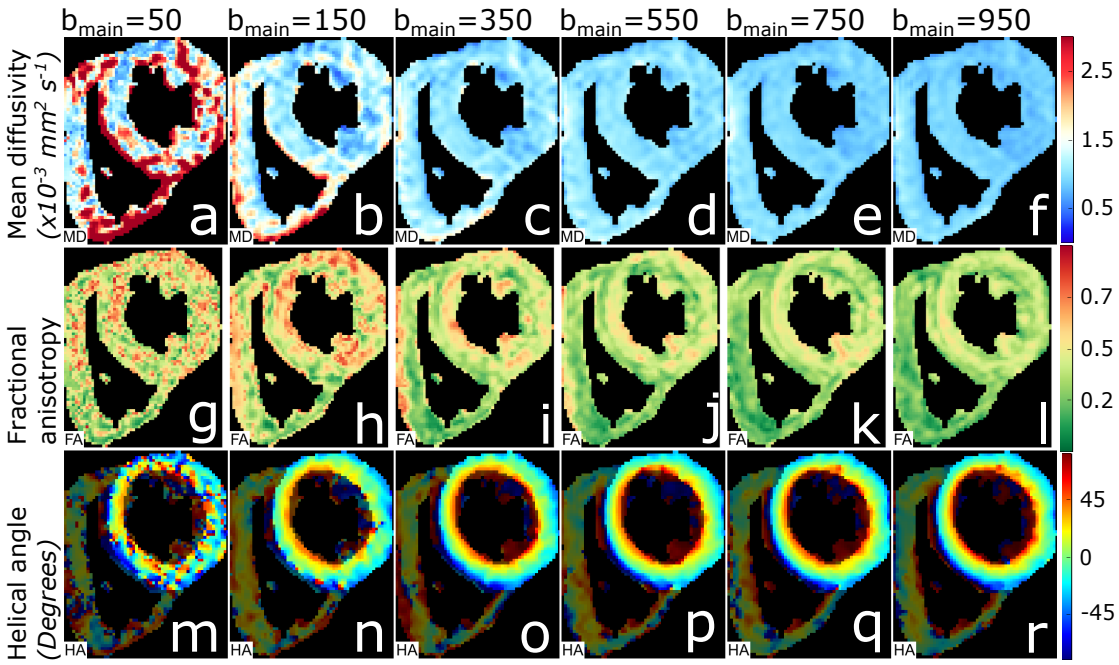

Figure 3: Example cDTI parameter maps (MD, FA and HA) from one example subject with b_{main} from 50 to 950 s mm^{-2}. In each case $bref_{15}$ was used as a reference. The b-values given are those prescribed (before heart rate correction) in units of s mm^{-2}. The shaded region in the HA maps indicates the areas excluded from the left ventricular region of interest.

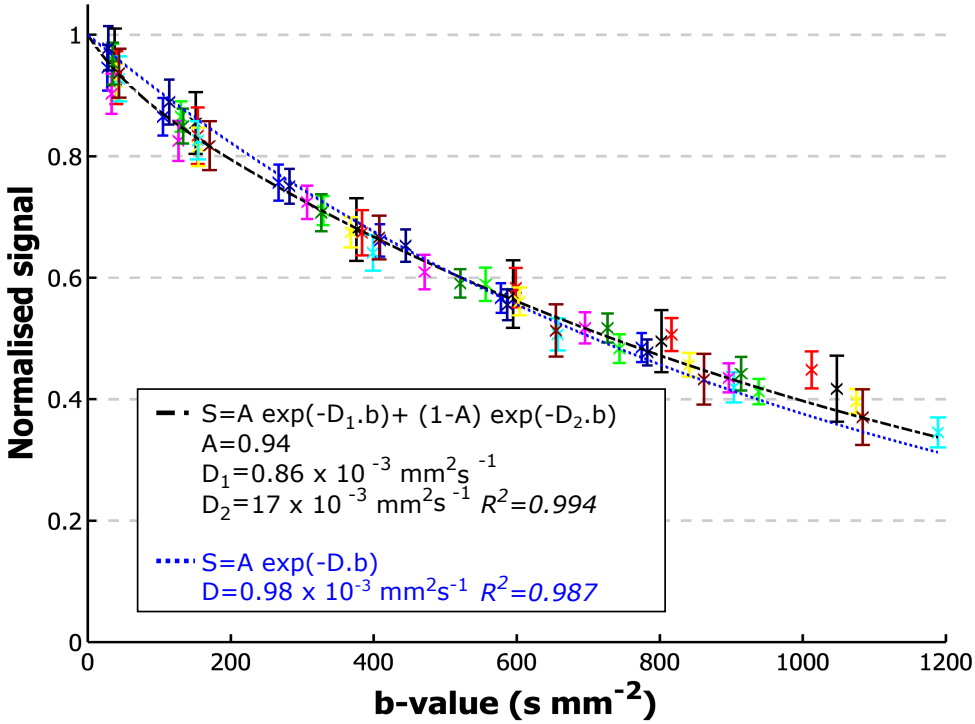

Figure 4: Normalised signal in the trace diffusion-weighted images plotted with the b-value (corrected for heart rate) with the mono and bi-exponential models fitted to the data.

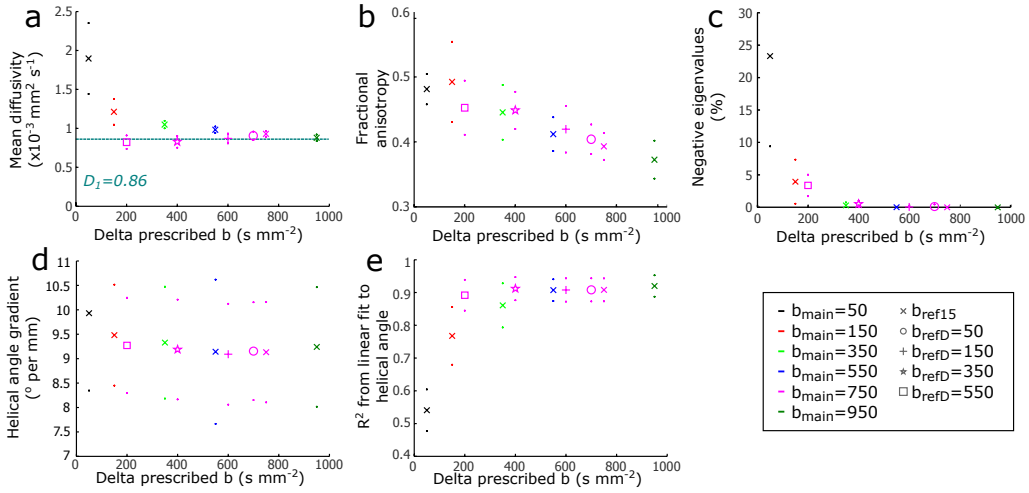

Figure 5: MD (a), FA (b), percentage of negative eigenvalues (c), transmural HA gradient (d) and the coefficient of determination (R^2) for the linear regression of transmural HA (e) derived using the 1AVE method and plotted with the difference in prescribed b_{main} and b_{ref} (defined as Δb in the text). For each parameter, the mean is plotted ± the standard deviation shown as small point markers. The main markers are colour coded by the b_{main} and the marker style indicates b_{ref}. The value of D_1 from the bi-exponential model described by equation 3 and calculated in figure 4 is shown on the plots of MD. The upper error markers for b_{main}=50 s mm^{-2} are not shown in parts c and d as the errors are large and lie far outside the displayed scale. Also see figure S2.

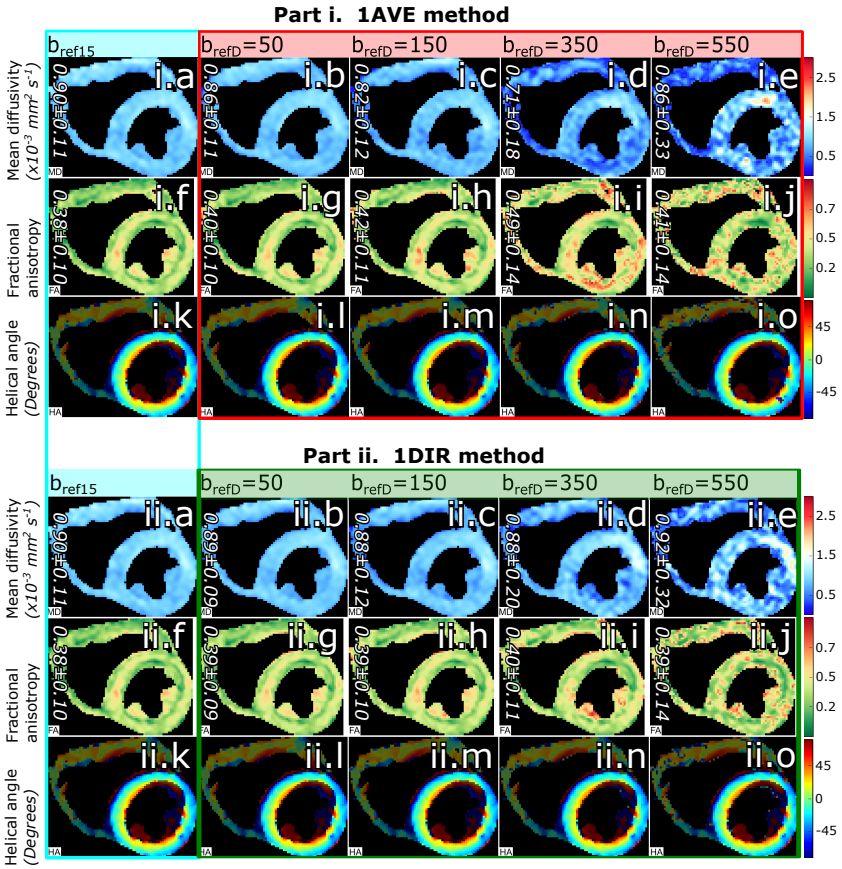

Figure 6: Example cDTI parameter maps calculated using a b_{main}=750 s mm^{-2} with increasing b_{ref}. Reference images were calculated using the 1AVE method (part i) and 1DIR method (part ii). The b_{ref15} images are the same in both cases. The mean ± standard deviation of the left ventricular MD and FA is shown on the corresponding images. The b-values given are those prescribed (before heart rate correction) in units of s mm^{-2}.

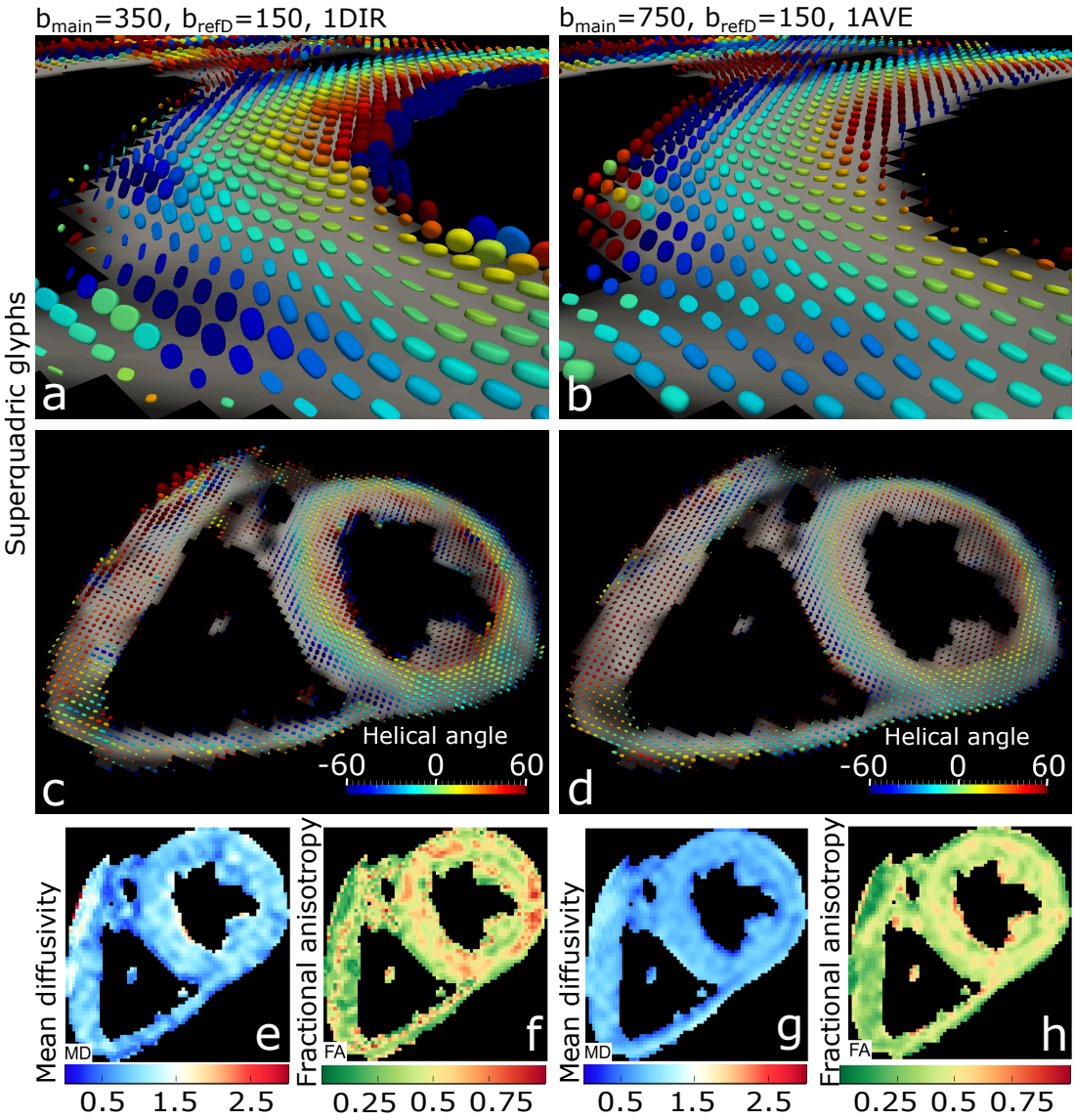

Figure 7: A comparison of the parameters closest to those used in our previous studies (b_{main}=350 and b_{refD}=150 s mm^{-2} using 1DIR) in the left hand column (a, c, e and f) and the proposed new protocol (b_{main}=750 and b_{refD}=150 s mm^{-2} using 1AVE) in the right hand column (b, d, g, h). Superquadric glyphs describing the full diffusion tensor in the lateral wall (a and b) and the full myocardium (c and d) are coloured by helical angle. MD in units of ×10^{-3} mm^2 s^{-1} (e and g) and FA (f and h) maps are also shown for each case. The b-values given are those prescribed (before heart rate correction) in units of s mm^{-2}.